Journal of Food Engineering 239 (2018) 92–103

Contents lists available at ScienceDirect

Journal of Food Engineering

journal homepage: www.elsevier.com/locate/jfoodeng

Effects of κ-carrageenan on the structure and rheological properties of fish gelatin

Li Cheng Sow[a,b], Jia Min Nicole Chong[a], Qiu Xu Liao[c], Hongshun Yang[a,b,*]

[a] Food Science and Technology Programme, c/o Department of Chemistry, National University of Singapore, 3 Science Drive 3, Singapore, 117543 Singapore
[b] National University of Singapore (Suzhou) Research Institute, 377 Lin Quan Street, Suzhou Industrial Park, Suzhou, Jiangsu 215123, PR China
[c] Anderson Junior College, 4500 Ang Mo Kio Ave 6, Singapore, 569843, Singapore

ARTICLE INFO

Keywords:
Fish gelatin
κ-Carrageenan
Atomic force microscopy
Confocal laser scanning microscope
Rheology
Nanostructure

ABSTRACT

Fish gelatin (FG) and κ-carrageenan (KC) were mixed to simulate the physicochemical properties of porcine gelatin (PG). The effects of the mixing ratio between FG and KC on the interaction, structure, and rheological properties of FG were investigated. The maximum associative interaction occurred at the critical mixing ratio of KC:FG (w/w) at 4:96, where the median particle size (D_{50}) of the FG-KC coacervates was 1168 ± 175 nm, and the zeta potential was −3.8 ± 0.8 mV. Interestingly, the rheological properties of the mixed gel (KC:FG at 4:96) matched those of PG, including the melting temperature (T_m), gelling temperature (T_g), dynamic consistency factor (K_f), and instantaneous compliance (J_0). The relationship between structure and physicochemical properties was proposed as a schematic model. The associative interaction between FG and KC was critical for FG's modification and could be applied to improve FG's rheological properties towards PG.

1. Introduction

Gelatin is a multifunctional food ingredient. Most marketed gelatin (> 98%) originates from mammalian sources, especially pigs and cattle (Karim and Bhat, 2009). But mammalian gelatin like porcine and bovine gelatin is not allowed for religious people such as Muslim, Jews, and Hindus (Haug et al., 2004). The physicochemical properties of fish gelatin (FG) including gel strength, melting and gelling temperature and rheological properties are poor compared to mammalian gelatin (Pang et al., 2017; Sow et al., 2017, 2018; Sow and Yang, 2015). To apply FG as a mammalian gelatin replacer, its physicochemical properties should be modified in order to match those of mammalian gelatin. The extraction of FG from seafood processing waste can also improve seafood sustainability and food security (Feng et al., 2017a, 2017b).

The physicochemical properties of FG could be modified by mixing FG with other food polysaccharides (Sow et al., 2017, 2018). For example, mixing with biopolymers resulted in either associative or segregative phase separation (Fang et al., 2006). Gelation further retarded phase separation, leading to complex structure, morphologies and mechanical properties (Cao et al., 2015).

κ-carrageenan (KC) is a negatively charged, sulphated polysaccharide from red seaweed (Yang et al., 2018), which is bioactive and rich in nature, with good biocompatibility (Kitade et al., 2017). KC has been widely applied in the food industry as a stabilizer, thickener, and gelling agent (Robal et al., 2017). Most previous studies used type B mammalian gelatin and KC (Cao et al., 2015; Derkach et al., 2015; Derkach et al., 2014; Fang et al., 2006; Voron'ko et al., 2016, 2017). These previous studies focused on the condition of the associative phase separation and the formation of complex coacervates (Fang et al., 2006; Voron'ko et al., 2017). The factors including temperature, pH, mixing ratio, salt type and concentration could affect the interaction between gelatin and KC. Electrostatic interaction, and to a less extent hydrogen bond and hydrophobic interaction could lead to the associative interaction between gelatin and KC (Voron'ko et al., 2017). Mixing of FG and KC was reported by Haug et al. (2004), where mixing of cold water FG (2%, w/v) and KC (1%, w/v) improved the melting (T_m) and gelling temperature (T_g) of FG and the formation of KC network was considered to contribute to the improved physicochemical properties. Furthermore, Pranoto et al. (2007) reported a dry film formed by tilapia FG (5%, w/v) and KC (2%, w/v) that had improved thermal and mechanical properties. However, these studies did not compare the KC-FG system to the mammalian gelatin.

The present study aimed to evaluate the possibility of using FG-KC mixed gel as a replacer for porcine gelatin (PG) and established the relationship of interaction-structure-physicochemical properties for FG-KC. The upper limit of the mixing ratio of KC:FG was fixed at 20:80 (w/w) to avoid over modification of FG into a new material. Confocal laser

* Corresponding author. Food Science and Technology Programme, c/o Department of Chemistry, National University of Singapore, 3 Science Drive 3, Singapore, 117543, Singapore.
E-mail address: chmynghs@nus.edu.sg (H. Yang).

https://doi.org/10.1016/j.jfoodeng.2018.05.035
Received 19 February 2018; Received in revised form 25 April 2018; Accepted 31 May 2018
Available online 14 June 2018

scanning microscope (CLSM) and atomic force microscope (AFM) were employed to investigate the structure at the micro and nano levels. Rheological tests were used to assess the modification of physicochemical properties of FG-KC gels. Moreover, creep-recovery study and Burgers model were applied to evaluate the deformation and relaxation properties of modified FG. To date, to our best knowledge, this approach has not been employed in mammalian gelatin replacement.

2. Materials and methods

2.1. Materials

Commercial tilapia FG (180 Bloom) was obtained from Jiangxi Cosen Biology Co., Ltd (Yingtan, Jiangxi, China) while PG was from Qingdao Huachang Food Ingredients Co. Ltd (Qingdao, Shandong, China). κ-Carrageenan (SeaKem® CM 611) was a gift from FMC Health and Nutrition (Philadelphia, PA, USA). The characteristics of the raw materials are shown in Table A1. The viscosity averaged molecular weight was determined from the intrinsic viscosity and Mark Houwink equation (Bohidar, 1998; Vreeman et al., 1980) while the counterions content was analysed using inductive coupled plasma-optical emission spectroscopy (ICP-OES). Fluorescent markers fluorescein isothiocyanate (FITC) and rhodamine B, potassium bromide (KBr) and dimethyl sulphoxide (DMSO), were purchased from Merck KGaA (Darmstadt, Germany).

2.2. Sample preparation

Liquid samples (0.5%, w/v) were prepared for turbidity, particle size, zeta potential, CLSM, and AFM analysis. Gel samples (6.67%, w/v) were used for rheological test and Fourier transform infrared spectroscopy (FTIR). FG and KC solutions were separately hydrated in deionised water for 2 h, followed by heating and stirring at 65 °C for 10 min until dissolved. The solutions were then mixed together with gentle stirring and heating for 30 min at 60 °C to achieve a ratio of KC:FG (w/w), according to Table 1. All prepared samples had a pH between 6.2 and 6.5, which was below the isoelectric point of FG (pH 7.52) (Sow et al., 2017).

2.3. Turbidity

The hot liquid samples prepared according to section 2.2 were cooled to 25 °C. The absorbance at 600 nm was recorded at 25 °C using a UV-1700 spectrophotometer (Shimadzu Corporation, Kyoto, Japan) and the turbidity (τ) was calculated using the following equation,

$$\tau = -\left(\frac{1}{L}\right)\ln\left(\frac{I}{I_0}\right) \quad (1)$$

where L is the optical path length (cm), I is the intensity of radiation transmitted, and I_0 stands for the intensity of the incident radiation (Sow et al., 2017).

Table 1
Mixing ratios (w/w) of fish gelatin and κ-carrageenan (FG-KC) and the actual concentrations used in the experiments.
*Selected samples were prepared to the concentration of 6.67% (w/v). The "-" indicates that the samples were not prepared into gel form thus the rheological test and Fourier Transform Infrared spectroscopy (FTIR) were not carried out.

Sample	Mixing ratio (w/w)		Actual concentration at 0.5% (%, w/v)		Actual concentration at 6.67% (%, w/v)*	
	FG	KC	FG	KC	FG	KC
FG	100	0	0.5000	0.0000	6.67	0.000
FGC1	99.5	0.5	0.4975	0.0025	6.63	0.033
FGC2	99	1	0.4950	0.0050	–	–
FGC3	98	2	0.4900	0.0100	6.53	0.133
FGC4	96	4	0.4800	0.0200	6.40	0.267
FGC5	92	8	0.4600	0.0400	6.13	0.533
FGC6	90	10	0.4500	0.0500	6.00	0.667
FGC7	80	20	0.4000	0.1000	–	–
KC	0	100	0.0000	0.5000	0.00	–

2.4. Particle size and zeta potential

The hot liquid samples (section 2.2) were diluted with hot deionised water to 0.01% (w/v) and cooled to 25 °C. The measurements of particle size and zeta potential were conducted using a NanoBrook Omni Particle Size and Zeta Potential analyser (Brookhaven Instruments, NY, USA) with dynamic light scattering (DLS) and phase analysis light scattering mode, respectively (Sow et al., 2017). DLS used a light scattering angle of 173° while for zeta potential Smoluchowski's model was applied.

2.5. CLSM

The fluorescently labelled samples were prepared according to a previous method with slight modifications (Razzak et al., 2016). Rhodamine B and FITC were used to label FG and KC, respectively. The excitation/emission wavelengths of the dyes were 495/525 nm and 543/580 nm for FITC and rhodamine B, respectively. FG and KC solutions were prepared separately; the pHs of FG and KC were adjusted to 10.5 and 8.5, respectively, to facilitate dye binding. The dye solution (2%, w/v) was dissolved in DMSO, and 25 μL was added into 100 mL samples (0.5%, w/v). Labelling was carried out at room temperature for 90 min. Thereafter, the pHs of FG and KC solutions were adjusted to original pH, and rhodamine B-labelled FG and FITC-labelled KC were mixed according to the ratios in Table 1. The samples were imaged at two concentrations, i.e. 0.5% (w/v) and 6.67% (w/v) to evaluate the condition of solution and gel, respectively. The 0.5% (w/v) mixture (20 μL) was pipetted onto a cover glass slide (0.13–0.16 mm thickness) while 0.3 ml of 6.67% (w/v) gel was filled into a cuvette. The samples were covered from light and stored overnight at 4 ± 2 °C. The microstructure was captured using an Olympus Fluoview FV 1000 confocal scanning unit (Tokyo, Japan) equipped with argon ion and Helium-Neon (HeNe) lasers. Images were taken at 60 × magnification (PlanApo 60×/1.0 WLSM 0.17) with water immersion. The images were processed using Fluoview Software (Olympus, Tokyo, Japan).

2.6. Rheological tests

Gelatin gels (6.67%, w/v) were prepared and subject to rheological measurements using an Anton Paar MCR 102 controlled-stress rheometer (Anton Paar, Graz, Austria). Hot solutions were poured onto the rheometer bottom plate, and a thin layer of corn oil was applied to the rim of the samples to prevent evaporation (Yang et al., 2018). The samples were subject to four protocols. The geometry used in protocol 1 to 3 was a stainless-steel cone plate of 60 mm diameter (angle: 1°, 0.1667 mm gap). Prior to the measurements, linear viscoelastic region (LVR) range was pre-determined based on the results of strain sweep (Fig. C2) and frequency sweep (Fig. 3A) at 10 °C. Detailed steps are as follows.

(1) The samples were maintained at 60 °C for 15 min and cooled to 10 °C and hold for 90 min at 10 °C (1% strain, 1 Hz frequency) (time sweep) for gel maturation. Changes in storage (G′) and loss (G″) modulus were recorded.
(2) After the gel set, a frequency sweep (0.1–100 Hz or angular frequency, ω of 0.6283–628.3 rad/s) at 1% strain was conducted. A power law relationship between ω and complex viscosity (η*) was applied to characterise the rheological properties (Nakauma et al., 2016),

$$\tau = -\left(\frac{1}{L}\right)\ln\left(\frac{I}{I_0}\right) \tag{2}$$

$$\eta^* = \frac{\sqrt{(G')^2 + (G'')^2}}{\omega} \tag{3}$$

where K_f is the dynamic consistency index, and n_f is the dynamic power law factor.

(3) A creep-recovery test was conducted by applying a constant shear stress of 200 Pa from 0 to 915.5 s (creep-phase). The stress was removed and the changes in strain were measured from 915.5 to 1820 s (recovery phase) (Fu et al., 2016). The compliance was processed by J(t) = γ/σ, where γ is the shear strain and σ is the shear stress of the creep phase. The compliance data were fitted to Burges model using Eq. (4) and Eq. (5) for creep and recovery phases, respectively.

$$J(t)_c = J_{0_c} + \sum_{i=1}^{3}\left[J_{m_{ic}}\left(1 - e^{\frac{-t}{\lambda_{ic}}}\right)\right] + \frac{t}{\eta_0} \tag{4}$$

$$J(t)_r = J_{max} - J_{0_r} - \sum_{i=1}^{3}\left[J_{m_{ir}}\left(1 - e^{\frac{-t}{\lambda_{ir}}}\right)\right] \tag{5}$$

where J_0, J_m, and J_{max} are instantaneous, viscoelastic, and maximum compliance, respectively; t and λ are time and retardation time, respectively, and η_0 is the zero-shear viscosity. The example of creep-recovery curve and illustration of Burgers model parameters is shown in Fig. B1.

(4) Gel-sol-gel transition was performed on gel samples (6.67%, w/v) that were prepared in Petri dishes at 4 ± 2 °C for 17 h. The gels were cut and placed on a pre-conditioned rheometer at 10 °C for 10 min, and a stainless-steel parallel plate geometry of 25 mm diameter was used with gap size of 0.8 mm. The gel was heated from 10 to 60 °C at 1 °C/min, and then cooled from 60 to 10 °C at a constant strain of 1% and frequency of 1 Hz. The temperatures at the crossover of G′ and G″ during heating and cooling process were recorded as the T_m and T_g, respectively (Sow et al., 2017).

2.7. AFM

The hot liquid samples (section 2.2) were diluted to 0.01% (w/v) using filtered deionised water. Then 20 µL sample was applied on a freshly cleaved mica surface and dried overnight in a clean, covered Petri dish before imaging. The image was collected using table top (TT)-AFM (AFM workshop, Signal Hill, CA, USA) equipped with an AppNano ACLA-10 probe (Applied NanoStructures, Mountain View, CA, USA) at resonance frequency of 160–225 kHz and force constant of 36–90 N/m. Vibrating mode (tapping mode) was employed and scanning was performed in air at ambient temperature. The images were processed using Gwyddion 2.45 (http://gwyddion.net); the bright and dark areas on the image represent the difference in the height of the features (Chen et al., 2018; Feng et al., 2016).

2.8. FTIR

The gel samples (6.67%, w/v) were freeze-dried, milled, mixed with KBr powder (3 mg sample/100 mg KBr), and pressed into a pellet. The samples were scanned for wavenumbers from 4000 cm^{-1} to 450 cm^{-1} using a Spectrum One FTIR spectrometer (PerkinElmer, Waltham, MA, USA) (Sow and Yang, 2015). The scan number was 64 and resolution was 4 cm^{-1}. Background spectra were registered before every sample scan. Pre-processing of the spectra including background removal, baseline correction, smoothing and normalisation, were conducted using Spectrum software. Amide I region (1600–1700 cm^{-1}) was deconvoluted, which was then fitted using Origin Pro 9 (OriginLab, Northampton, MA, USA).

2.9. Statistical analysis

Each experiment was repeated at least three times, with at least duplicate measurements performed within each run. The results are expressed as the mean ± standard deviation. Statistical differences within and between test groups were determined using one-way ANOVA ($P < 0.05$) and Duncan's multiple range test by the SPSS Statistics 20 software (IBM, Chicago, IL, USA). For imaging, at least a dozen of parallel images were recorded and analysed.

3. Results and discussion

3.1. Turbidity, particle size, and zeta potential

The interaction between FG and KC was investigated based on the changes of turbidity, particle size, and zeta potential (Fig. 1). The FG and KC solutions were clear, and the median particle sizes (D_{50}) of FG and KC were 200.2 ± 58.6 and 995.5 ± 229.0 nm, respectively. From the zeta potential (Fig. 1C), KC was strongly negatively charged (−57.9 ± 9.2) while FG was weakly positive (9.2 ± 1.3 mV). The FG and KC mixtures at KC:FG ratio from 0.5:99.5 to 4:96) showed

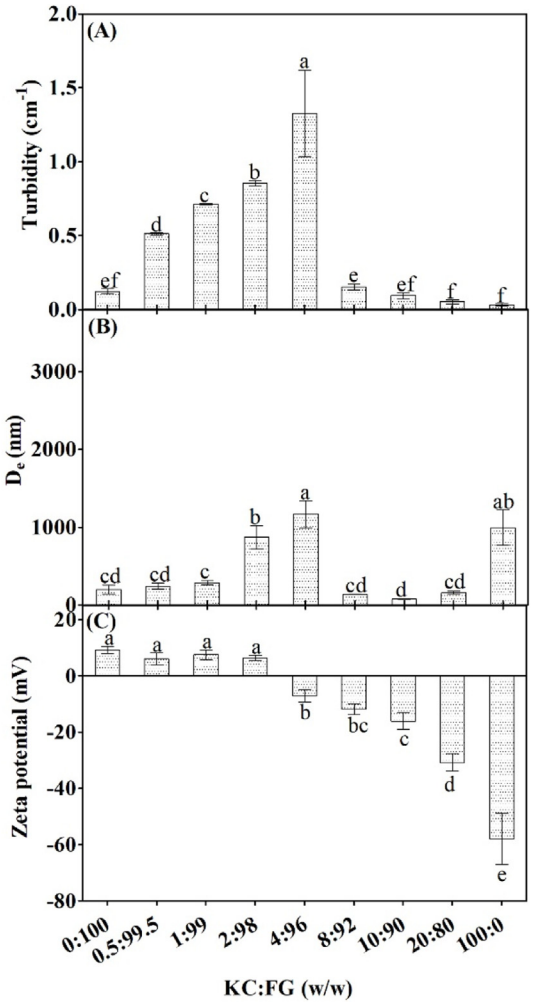

Fig. 1. Effect of the κ-carrageenan and fish gelatin (KC: FG) mixing ratio on turbidity, particle size (D_{50}), and zeta potential of the mixtures (0.5%, w/v). *Within each property, means with different lowercase letters are significantly different ($P < 0.05$) among different groups.

increased turbidity and particle size (Fig. 1A and B), which reached a maximum at KC:FG (w/w) ratio of 4:96 (FGC4). The greatest D_{50} of FGC4 observed was 1168 ± 175 nm. Derkach et al. (2014) reported a polyelectrolyte complex of type B gelatin and KC with a particle size of 1400 nm. Interestingly, the FG-KC mixture showed decreasing zeta potential as the KC ratio increased. At KC:FG (w/w) of 2:98 (FGC3) and 4:96 (FGC4), the zeta potential was close to neutral (6.3 ± 0.9 to −7.1 ± 2.2 mV), indicating that most of the positively charged surfaces of FG were bound by KC. These results showed that the associative interaction between the positively charged FG and negatively charged KC was electrostatically driven. The current results are consistent with the reports of Fang et al. (2006) which reported an electrostatic associative interaction in a type B gelatin-KC mixture and Haug et al. (2004) which reported increased turbidity during associative phase separation of KC and cold water FG.

Further increasing the KC:FG (w/w) ratio from 8:92 to 20:80 decreased the turbidity and particle size significantly, as the mixtures were solely negatively charged. Increasing KC ratio also increased the opportunity for intermolecular KC interaction. When the temperature decreased from 60 to 25 °C, the KC random coils underwent molecular ordering process to form double helices (Yang et al., 2018), resulting in segregative FG-KC interaction (Fang et al., 2006). For the associative FG-KC complexes, they may form initially, followed by segregative interaction in the biopolymer-depleted phase because of KC molecular ordering. This situation was described as “associative-co-segregative region” (Fang et al., 2006).

3.2. CLSM

To confirm whether the FG-KC system was completely segregative, or some amount or small size of complex coacervates were still present when KC:FG was above 4:96, microstructures of selected FG-KC mixtures (FGC1, FGC3, FGC4, FGC6), and FG and KC alone were studied using CLSM (Fig. 2). Both the solution (0.5%, w/v) and gel (6.67%, w/v) samples were examined. The microstructures of KC and FG were homogenous, with some crystalline structure in KC (Fig. 2A, G) and spherical aggregates in FG (Fig. 2B, H). At a high ratio of FG (99.5%) in FGC1, the microstructure showed many FG-like features that were mostly red spherical aggregates (Fig. 2C, I). Interestingly, the gel samples showed a higher density of aggregates (Fig. 2I) than the solution samples (Fig. 2C). When the KC ratio increased, a cloud-like structure developed in FGC3 (Fig. 2D), which was further developed into densely interconnected aggregates in FGC4 (Fig. 2E). The yellowish colour of the dense aggregates indicated that the structures were formed by both FG (red) and KC (green), resulting in obvious contrast to the background. Compared with the report of Fang et al. (2006), the high contrast cloud-like structures were associative coacervates. At gel state, spherical complex coacervates were identified in FGC3 and FGC4 (Fig. 2J and K). As a comparison, FGC6 showed an associative-co-segregative structure (Fig. 2F, L), where segregated FG aggregates (red) were found superimposed on continuous KC (green) background, and the yellowish aggregates may result from FG-KC association in gel state (Fig. 2L).

3.3. Rheology

For the rheological tests, 6.67% (w/v) gel, which is the standard concentration used to evaluate gelatin texture properties, was prepared (Karim and Bhat, 2009). PG (240 Bloom) was used as the reference.

The G′ and G″ increased continuously and approximated to a plateau when the gel was stored for 90 min at 10 °C (Fig. A1). The moduli at the end of the time sweep (90 min) at 10 °C were compared (Table 2). G′ of FGC4 was similar to PG at the end of the time sweep (5692 ± 334 Pa *vs.* 5525 ± 458 Pa). For all samples the G′ was at least 100 times greater than G″, a typical characteristic of strong gel system (Yang et al., 2018). The addition of KC increased G′ and G″, except FGC1 and FGC3. Previously, when carrageenan was mixed with whey protein isolate, a negative effect on G′ was found. The reason may be that the protein-polysaccharide interaction inhibited the network formation of milk gel (Pang et al., 2016). While mixing ratios of KC:FG were greater than 4:96 (w/w) (FGC4, FGC5, and FGC6), significant increases in G′ and G″ were observed. This might be because excess KC may self-associate, contributing to the increased G′ and G″, as reported by Haug et al. (2004).

Frequency sweep was performed on the gel sample at 10 °C (Fig. 3) to compare the mechanical strength of the hydrogel (Anvari and Chung,

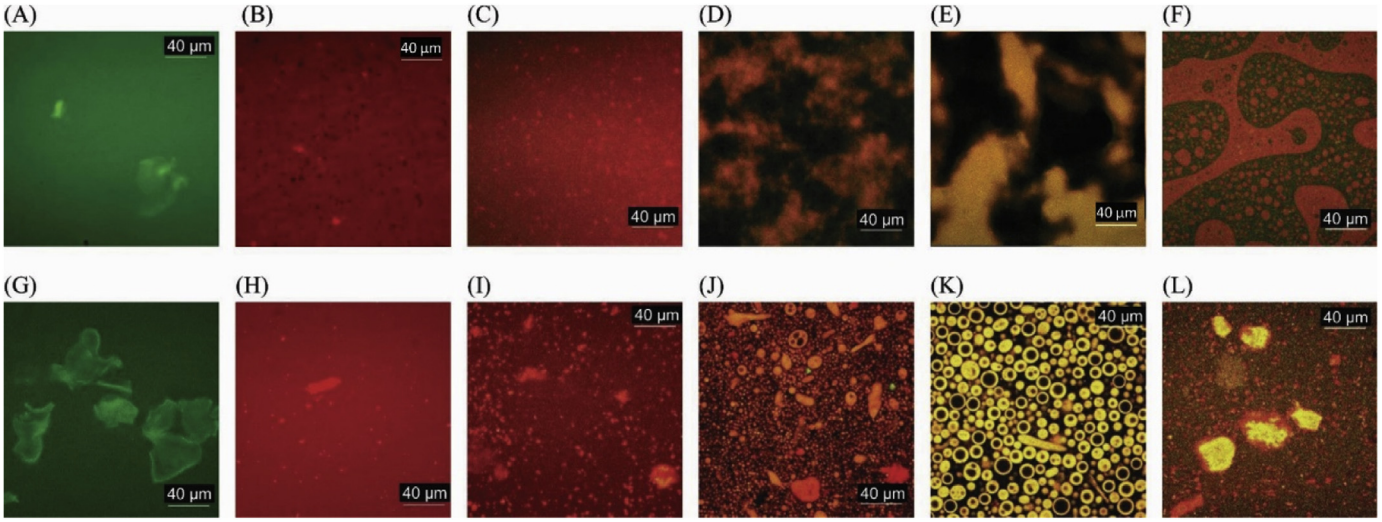

Fig. 2. Microstructure of 0.5% (w/v) solution (A–F) and 6.67% (w/v) gel (G–L) of (A, G) κ-carrageenan (KC); (B, H) fish gelatin (FG) and FG-KC mixtures having different mixing ratios (KC: FG, w/w): (C, I): 0.5: 99.5 (FGC1); (D, J): 2: 98 (FGC3); (E, K): 4: 96 (FGC4) and (F, L): 10: 90 (FGC6).
*The images were obtained from samples prepared at 0.5% (w/v); fluorescein isothiocyanate (FITC, green) was used to stain KC while rhodamine was used to stain FG (red). (For interpretation of the references to colour in this figure legend, the reader is referred to the Web version of this article.)

Table 2
Storage (G′) and loss (G″) modulus at the end of time sweep (90 min, 10 °C), rheological parameters of frequency sweep fitting (Eq. (2)), as well as the melting temperature (T_m) and gelling temperature (T_g) determined from the temperature sweep test.

*Within each column, means with different lowercase letters are significantly different ($P < 0.05$) among different groups.

*R^2 for the fitting of the frequency sweep results to Eq. (2) for all the samples was greater than 0.9999.

Sample	Time sweep		Frequency sweep		Temperature sweep	
	G′ (Pa)	G″ (Pa)	$n_f \times 10^{-2}$	$K_f \times 10^3$ (Pa·s$^{(1-n_f)}$)	T_m (°C)	T_g (°C)
PG	5692 ± 334^{c}	51 ± 5de	99.40 ± 0.02^{a}	5.64 ± 0.33^{c}	32.17 ± 0.21^{bc}	23.62 ± 0.13^{b}
FG	5114 ± 113de	57 ± 2de	99.25 ± 0.25^{b}	4.56 ± 0.66^{d}	27.78 ± 0.45^{e}	18.89 ± 1.50^{c}
FGC1	3523 ± 388^{f}	42 ± 4^{e}	98.88 ± 0.19^{bc}	3.48 ± 0.37^{e}	29.13 ± 0.02^{d}	18.21 ± 0.09^{c}
FGC3	4220 ± 207^{e}	85 ± 11^{d}	98.60 ± 0.35^{c}	4.14 ± 0.19^{de}	29.49 ± 0.64^{cd}	19.28 ± 0.21^{c}
FGC4	5525 ± 458^{cd}	121 ± 19^{c}	98.51 ± 0.39^{c}	5.54 ± 0.56^{c}	30.50 ± 0.48^{c}	20.44 ± 0.01^{bc}
FGC5	9016 ± 755^{b}	286 ± 32^{b}	97.74 ± 0.18^{d}	9.33 ± 0.62^{b}	33.13 ± 0.12^{b}	27.19 ± 0.14^{a}
FGC6	11139 ± 401^{a}	362 ± 1^{a}	97.69 ± 0.07^{d}	10.77 ± 0.41^{a}	35.42 ± 0.31^{a}	26.04 ± 0.36^{a}

2016). Fig. 3A and B shows that both G′ and G″ increased with increasing frequency. In addition, G′ was more weakly dependent on frequency than G″, indicating a solid-like rheological property (Zhong and Ikeda, 2012). The changes in η* during the frequency sweep are shown in Fig. 3C. The gel exhibited shear thinning behaviour, where η* decreased linearly with increasing frequency (Fig. 3C) (Anvari and Chung, 2016). The results fitted well with the power law model (Eq. (2)), with $R^2 > 0.99$ for all samples. Table 2 shows the specific parameters. The n_f decreased when KC increased in the mixture, while K_f increased with increasing KC. When n_f is equal to 1, the system is completely elastic. However, when n_f is 0, the system is completely viscous (Nakauma et al., 2016). The decrease in n_f indicated that a high level of KC (KC:FG > 4:96, w/w) modified the rheological properties of FG by increasing the viscous characteristic of the gel. The FG-KC gel was more frequency dependent as K_f increased. The higher frequency dependence of FGC 5 & FGC6 gel also indicated that the gel structure became looser at greater oscillatory shear and frequency (Anvari and Chung, 2016). Among all the samples, the response of FGC4 to the frequency sweep was similar to PG, with a similar K_f (5.64 ± 0.33 (PG) *vs.* 5.54 ± 0.56 (FGC4)).

In creep-recovery test (Fig. 3D), a small amount of KC (FGC1, FGC3) increased the compliances, while a high ratio of KC (FGC5, FGC6) decreased it significantly. An increase in compliance indicates that the gel has a strong and stiff structure capable of resisting deformation (Fu et al., 2016). The results of creep-recovery tests were further fitted into Burgers model (Eqs. (4) and (5)) which combines Kelvin and Maxwell models and is widely used to characterise elastic and viscous properties of food products (Fu et al., 2016; Moreira et al., 2010; Yilmaz et al., 2012). The corresponding parameters of Burgers model for creep phase and recovery phase of the current study are presented in Tables 3 and 4, respectively.

J_0 and J_{max} are related to the rigidity and firmness of gel network (Fu et al., 2016; Messens et al., 2000). Yilmaz et al. (2012) reported a strong negative correlation between J_{max} and hardness/chewiness. J_0 and J_{max} in both creep and recovery phase increased in FGC1 & FGC3 compared with FG; however, they decreased in FGC4, FGC5, and FGC6. There were no significant differences ($P > 0.05$) between the J_0 and J_{max} of PG and FGC4 (Tables 3 and 4). The viscoelastic compliance, $J_m(J_{m_1}, J_{m_2}, J_{m_3})$ was observed to increase in FGC1 and FGC3 compared to that of FG, indicating that the gel became less solid-like (Messens

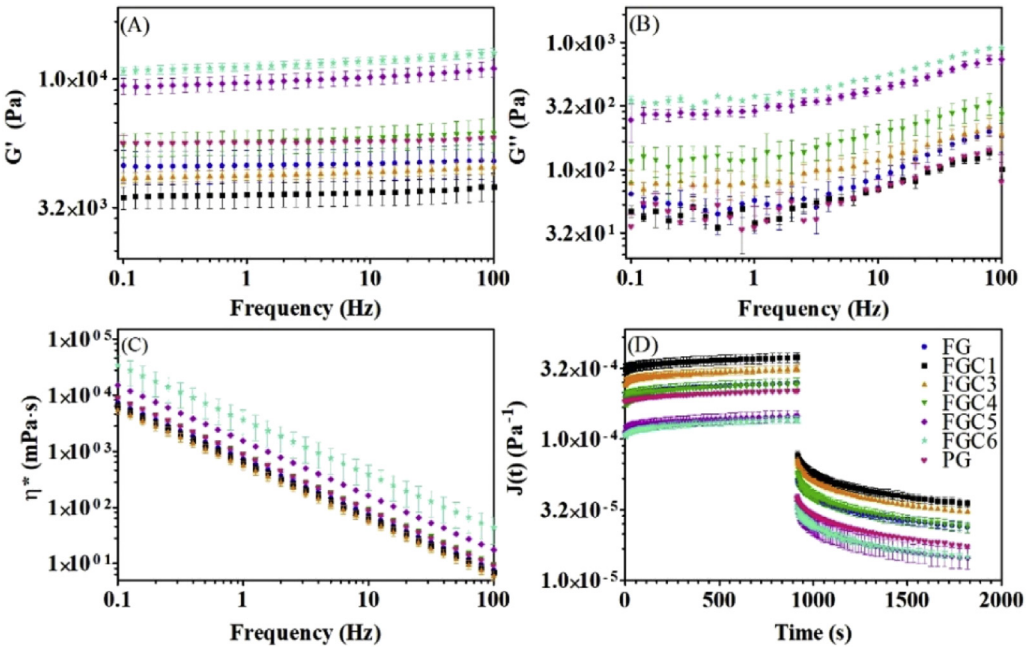

Fig. 3. Frequency sweep results of (A) storage modulus, G′; (B) loss modulus, G″; (C) complex viscosity, η*; and creep-recovery compliance (J(t)) of fish gelatin (FG), FG- κ-carrageenan (KC) mixtures and porcine gelatin (PG) gel (6.67%, w/v). *FGC1, FGC3, FGC4, FGC5, and FGC6 refer to the FG-KC mixtures with mixing ratios (KC:FG, w/w) of 0.5:99.5, 2:98, 4:96, 8:92, and 10:90, respectively.

Table 3
Parameters of Burgers model from the creep phase (0–915.5 s).
*Within each column, means with different lowercase letters are significantly different ($P < 0.05$) among different groups.

Sample	$J_0 \times 10^{-5}$ (Pa^{-1})	$Jm_1 \times 10^{-5}$ (Pa^{-1})	Jm_2 x 10^{-5} (Pa^{-1})	Jm_3 x 10^{-5} (Pa^{-1})	λ_1 (s)	λ_2 (s)	λ_3 (s)	η_0 x 10^7 (Pa·s)	R^2
PG	18.5 ± 0.1^{d}	1.47 ± 0.06^{cd}	0.44 ± 0.02^{d}	0.25 ± 0.04^{e}	238 ± 5^{ab}	37.2 ± 9.6^{a}	4.08 ± 1.06^{a}	5.86 ± 0.21^{b}	0.99991
FG	20.1 ± 0.1^{c}	1.83 ± 0.07^{bc}	0.62 ± 0.03^{c}	0.31 ± 0.08^{de}	241 ± 8^{a}	32.0 ± 1.0^{ab}	3.21 ± 0.53^{abc}	4.39 ± 0.01^{c}	0.99997
FGC1	30.7 ± 0.2^{a}	2.69 ± 0.02^{a}	0.80 ± 0.03^{b}	0.64 ± 0.01^{ab}	211 ± 47^{abc}	23.3 ± 10.4^{bc}	2.03 ± 1.35^{cd}	2.92 ± 0.52^{d}	0.99996
FGC3	24.8 ± 0.2^{b}	2.45 ± 0.21^{a}	0.92 ± 0.07^{a}	0.70 ± 0.14^{a}	217 ± 3^{abc}	25.1 ± 1.9^{bc}	2.77 ± 0.17^{bcd}	3.37 ± 0.14^{cd}	0.99996
FGC4	18.9 ± 0.2^{d}	2.00 ± 0.15^{b}	0.76 ± 0.05^{b}	0.54 ± 0.04^{bc}	189 ± 9^{c}	19.8 ± 0.8^{c}	1.78 ± 0.41^{d}	4.00 ± 0.28^{cd}	0.99993
FGC5	11.0 ± 0.9^{e}	1.25 ± 0.15^{d}	0.48 ± 0.04^{d}	0.47 ± 0.05^{c}	192 ± 44^{bc}	22.9 ± 7.1^{bc}	2.46 ± 0.03^{bcd}	6.75 ± 1.67^{ab}	0.99995
FGC6	10.3 ± 0.4^{e}	1.30 ± 0.09^{d}	0.53 ± 0.06^{cd}	0.44 ± 0.05^{cd}	205 ± 13^{abc}	22.4 ± 1.3^{bc}	2.24 ± 0.22^{cd}	7.29 ± 0.77^{a}	0.99995

Table 4
Parameters of Burgers model from the recovery phase (915.5–1820 s).
*Within each column, means with different lowercase letters are significantly different ($P < 0.05$) among different groups.

Sample	$J_{max} \times 10^{-5}$ (Pa^{-1})	$J_0 \times 10^{-5}$ (Pa^{-1})	$Jm_1 \times 10^{-5}$ (Pa^{-1})	$Jm_2 \times 10^{-5}$ (Pa^{-1})	$Jm_3 \times 10^{-5}$ (Pa^{-1})	λ_1 (s)	λ_2 (s)	λ_3 (s)	R^2
PG	22.2 ± 1.3^{c}	18.2 ± 1.1^{c}	1.04 ± 0.05^{c}	0.44 ± 0.04^{c}	0.25 ± 0.00^{c}	216 ± 24^{a}	34.4 ± 0.9^{a}	3.05 ± 0.55^{a}	0.9999
FG	24.9 ± 0.1^{c}	19.7 ± 0.0^{c}	1.41 ± 0.11^{b}	0.54 ± 0.08^{bc}	0.40 ± 0.01^{bc}	219 ± 4^{a}	33.4 ± 2.40^{a}	2.96 ± 0.10^{a}	0.9999
FGC1	37.9 ± 3.1^{a}	30.2 ± 2.6^{a}	1.95 ± 0.11^{a}	0.88 ± 0.19^{a}	0.63 ± 0.08^{a}	218 ± 19^{a}	40.2 ± 13.4^{a}	4.18 ± 1.21^{a}	0.9999
FGC3	31.5 ± 1.8^{b}	24.1 ± 1.6^{b}	1.97 ± 0.69^{a}	0.94 ± 0.12^{a}	0.68 ± 0.18^{a}	211 ± 56^{a}	29.4 ± 11.4^{a}	2.62 ± 0.98^{a}	0.9999
FGC4	24.4 ± 2.5^{c}	18.6 ± 2.1^{c}	1.58 ± 0.21^{b}	0.75 ± 0.06^{ab}	0.61 ± 0.08^{ab}	225 ± 18^{a}	34.7 ± 6.3^{a}	3.49 ± 0.50^{a}	0.9999
FGC5	14.6 ± 1.4^{d}	10.9 ± 0.9^{d}	1.06 ± 0.12^{c}	0.59 ± 0.12^{bc}	0.48 ± 0.04^{ab}	291 ± 51^{a}	41.9 ± 0.8^{a}	3.67 ± 0.70^{a}	0.9998
FGC6	13.8 ± 0.8^{d}	10.1 ± 0.5^{d}	1.01 ± 0.12^{c}	0.47 ± 0.08^{c}	0.40 ± 0.00^{bc}	173 ± 13^{a}	21.6 ± 2.7^{a}	2.36 ± 0.24^{a}	0.9999

et al., 2000). In addition, J_{m_1} and J_{m_2} of FGC5 and FGC6 were decreased to the level of PG, indicating that the gel became more solid like and less viscoelastic. For η_0, a parameter representing the resistance to flow (Fu et al., 2016), it was reduced by low level KC especially when KC:FG ratio was below 4:96, but increased when KC level increased, which modified the viscous component of the FG gel.

The T_m and T_g were determined from the temperature sweep during the gel-sol-gel transition (Table 2). Addition of KC increased the T_m, and the increment in T_g became significant in FGC4, FGC5, and FGC6. Among the samples, the T_m (30.5 ± 0.48 °C) and T_g (20.44 ± 0.01 °C) of FGC4 matched those of PG (32.17 ± 0.21 °C and 23.62 ± 0.13 °C, respectively). Even though the concentrations of KC in FGC4 to FGC6 (0.267%–0.667%, w/v, Table 1) were below the gelation concentration (results not shown), it was able to improve the T_m, T_g, and the modulus, suggesting a phase-separated bi-continuous network instead of an interpenetrating network could have formed with increasing KC (Du et al., 2016). This produced a FG-KC mixed gel that was not the result of a simple additive behaviour of FG and KC. It was reported that the T_g of 1.5% (w/v) potassium form KC was 31 °C and T_m was 58 °C (Robal et al., 2017). Thus, when temperature decreased, a KC network could form before FG network (T_g = 18.89 ± 1.5 °C), possibly leading to a bi-continuous network. For FGC5 and FGC6, since they contained excess KC, they showed a significant increase of T_m and T_g that were even greater than PG.

Interestingly, the rheological properties suggested that the mixing ratio of KC:FG (w/w) at 4:96 (FGC4) was the critical point for significant changes of FG rheological property. At this critical mixing ratio, the maximum complex coacervation of FG-KC also formed (sections 3.1 & 3.2). Similar results were reported by Derkach et al. (2014, 2015), in which mixing of type B gelatin and KC at a ratio of 90:10 in a 2% (w/v) gel resulted in polyelectrolyte complex that showed significant modification of gelation rate, T_m, yield stress and G′. In the current study, the association complex coacervates of FG-KC could therefore improve the FG rheological properties, an outcome that is useful to prepare modified FG as replacer of PG.

3.4. Schematic model

Based on the results of interaction (*3.1*), microstructure (*3.2*) and rheological properties (*3.3*), a schematic model was proposed (Fig. 4) to demonstrate the modification of FG by KC. Oppositely charged FG and KC could associate together upon mixing, via an electrostatic interaction between OSO_3^- of KC and $NH_3^+$of lysine, hydroxylysine, histidine, and arginine residues of FG (Derkach et al., 2014). When the ratio of KC:FG was low (FGC1, FGC3), the unbound FG was in excess, resulting in insufficient complex coacervate formation which compromised the FG gel's rheological properties. However, when KC:FG ratio was increased to the critical ratio (4:96), large complex coacervates were formed and the formed aggregations contributed to the network strength of FG. When the ratio was further increased to above the critical ratio, significant modification of FG rheological properties occurred. Because in addition to complex coacervates of KC-FG, excess KC could contribute to additional strength to the gel network and to the formation of bi-continuous gel which contained separate FG network and KC network regions. In addition, the small particle size (Fig. 1B) developed above critical KC:FG ratio might also contribute to the pronounced rheological effects as the smaller particles can resist more deformation (van Riemsdijk et al., 2010) and aggregate into a denser network (Sow et al., 2017). Thus, above the critical KC:FG ratio, the rheological characteristics of KC became obvious, which had a high level of viscous component (G″, η_0) compared with gelatin that was more elastic.

3.5. Validation of the schematic model

3.5.1. AFM

Nanostructures of diluted samples (0.01%, w/v) were investigated by AFM to validate the proposed schematic model (Fig. 4). AFM provides direct structural visualisation at the nanoscale, and help illustrate the gelatin's aggregation behaviour which is related to the macroscale properties (Liu and Wang, 2011). Fig. 5A and B shows that FG alone presented homogenous structures comprising small spherical

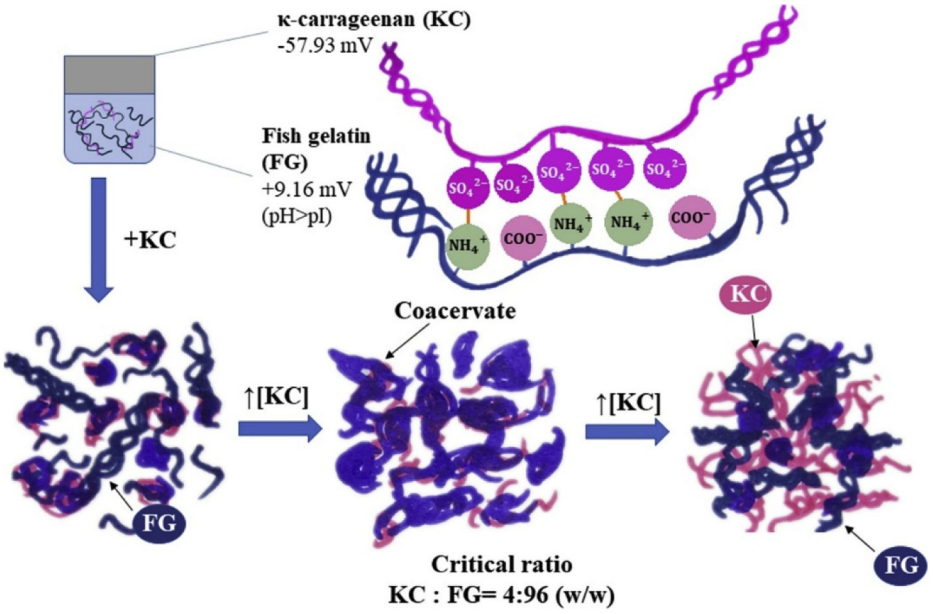

Fig. 4. Schematic model demonstrating the effect of κ-carrageenan (KC, pink) addition on the modification of fish gelatin (FG, blue) structure below critical mixing ratio of KC: FG (w/w) at 4:96, at the critical ratio (coacervates formation) and above the critical ratio (bi-continuous network). (For interpretation of the references to colour in this figure legend, the reader is referred to the Web version of this article.)

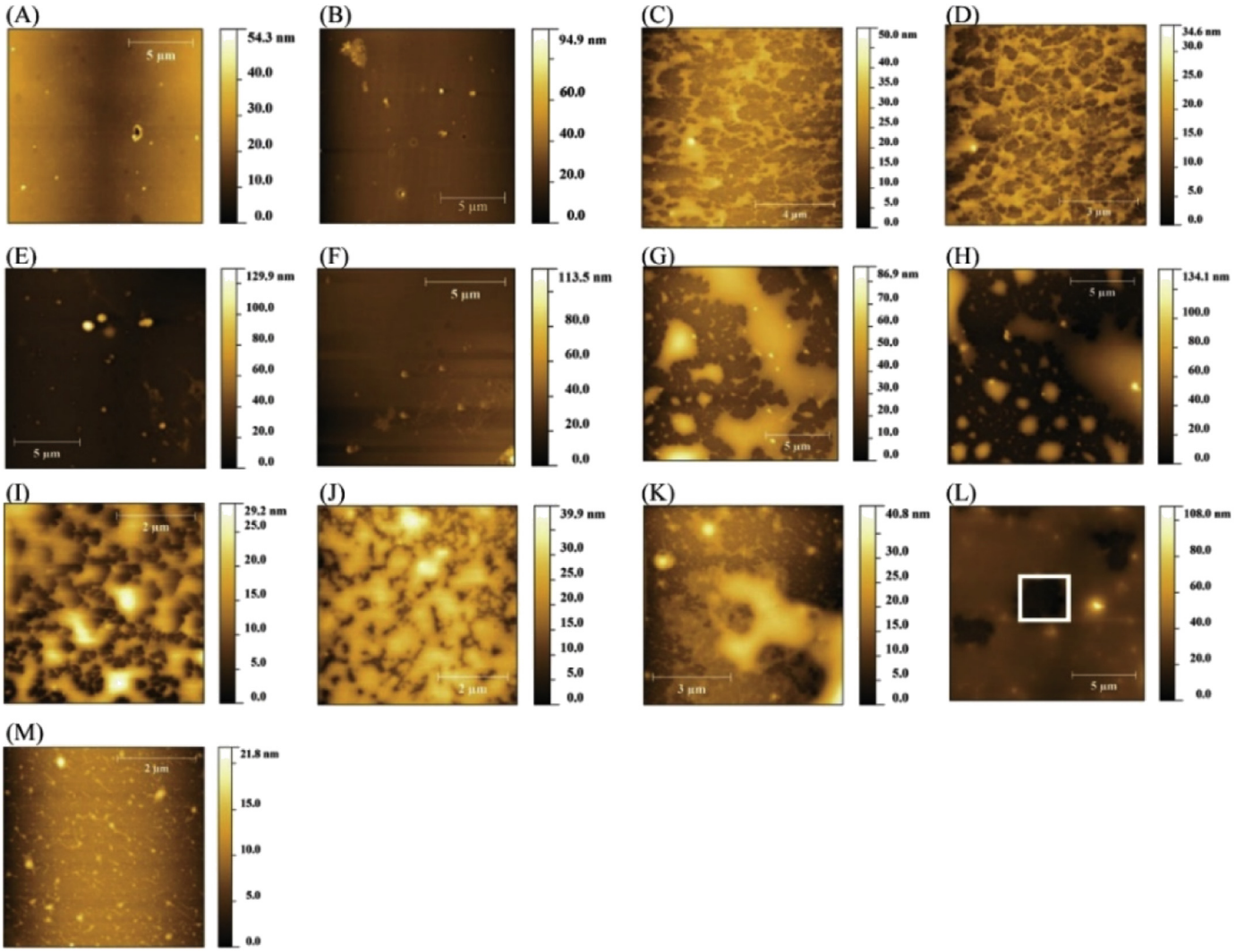

Fig. 5. Nanostructure of (A, B) fish gelatin (FG); (C, D) κ-carrageenan (KC); and the FG-KC mixtures at different mixing ratios (KC:FG, w/w) of (E, F) 0.5:99.5 (FGC1); (G, H) 2:98 (FGC3) and (I, J) 4: 96 (FGC4); (K, L, M) 10:90 (FGC6) featuring bi-continuous phase comprising (K, L) a complex coacervates region and (M) thin fibril structure underneath the dense region (white square) of (M). *The images were obtained from samples prepared at 0.01% (w/v) of KC-FG mixture.

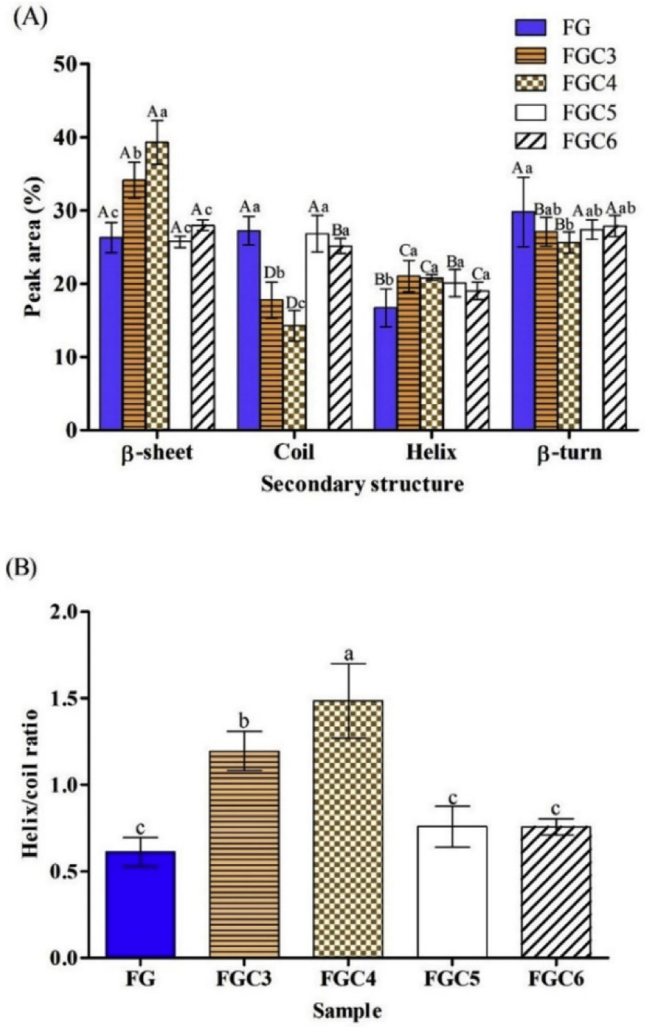

Fig. 6. Secondary structure of fish gelatin (FG) and selected FG- κ-carrageenan (KC) mixtures estimated from deconvolution of amide I spectra (A) relative peak area (%) and (B) ratio of helix-to-coil.
*Within each secondary structure, groups with different lowercase letters have significant statistical difference ($P < 0.05$). For the same sample, groups with different capital letters have a significant statistical difference ($P < 0.05$) among different size ranges.
* FGC3, FGC4, FGC5, and FGC6 refer to the FG-KC mixture with mixing ratio (KC:FG, w/w) of 2:98, 4:96, 8:92, and 10:90, respectively.

aggregates and annular pores, similar to previous reports (Sow et al., 2017, 2018; Sow and Yang, 2015; Wang et al., 2008). For KC, an interconnected porous fibrous network was observed (Fig. 5C and D). Yang et al. (2018) also reported that KC formed an interconnected cell wall-like, porous structure with large voids in between under field emission scanning electron microscopy. With low amount of KC in FGC1, the nanostructure resembled that of FG, with a few spherical aggregates (Fig. 5E) and some irregular aggregates (Fig. 5F). Complex coacervates in FGC3 and FGC4 were obvious (Fig. 5G–J) while the bi-continuous structure was found in FGC6 (Fig. 5K and L). In FGC6, there were also dense complex coacervates regions, and in the void region, thin fibril structures of KC were observed (Fig. 5M). These results were consistent with the CLSM microstructure (Fig. 2I and J). The nanostructures of FGC1, FGC4, and FGC6 agreed well with the schematic model, which further confirmed that the critical ratio of KC:FG was 4:94 as for FGC1, FGC4, and FGC6 the KC:FG was below the critical ratio, at the critical ratio and above the critical ratio, respectively.

3.5.2. FTIR

The amide I band (1600–1700 cm^{-1}) from FTIR results from vibration of C=O and C=N is useful to characterise protein secondary structure (Sow et al., 2017; Sow and Yang, 2015). The modification on the secondary structure of FG by KC was determined from amide I (1600-1700 cm^{-1}) deconvolution and peak fitting ($R^2 > 0.999$) (Fig. 6). The modification included increased β-sheets (1617–1642 cm^{-1}) and decreased random coils (1646–1652 cm^{-1}) in FGC3 & FGC4. The helix structure (1659–1662 cm^{-1}) increased while the β-turn structure (1672–1691 cm^{-1}) decreased in all the modified FGs compared to FG alone. KC addition might induce structural modification of FG by increasing the β-sheet structure that presented a large surface area for FG-KC association, a result similar to the pea protein-gum Arabic complex reported by Chourpa et al. (2006). FGC3 and FGC4 showed increased helix/coil ratio compared with FG (Fig. 6B). Coil to helix formation is the gelling mechanism for FG; therefore, the helix/coil ratio serves as an estimation of the triple helix content. The increased triple helix structure in FGC4 could promote the strength of the network. When KC was increased beyond the critical ratio (4:96, w/w), the helix/coil ratio reverted to the level of FG. This further supported the changes in rheological properties of FGC5 and FGC6 caused by the formation of KC-KC network.

4. Conclusion

Positively charged FG associated with negatively charged KC via electrostatic interactions. The critical mixing ratio between KC and FG was found to be 4:96 (w/w). At this critical ratio, the size of the complex coacervates was the greatest (1168 ± 175 nm) and the rheological properties of the FG gel were modified significantly, leading to similar properties as PG in terms of firmness (J_0), T_m and T_g. However, above the critical mixing ratio, excess KC self-associated and contributed to the segregation of the FG-KC mixture. Thus, the FG-KC interaction was changed from associative to more segregative, and the turbidity and particle size of the mixture decreased drastically. In addition, the rheological properties were modified to have enhanced viscous properties and firmness that were significantly different from PG, making this modification not suitable to be used as appropriate PG replacer. Structurally, the complex coacervates formed were visualised by CLSM and AFM. The structure study supported the property change and the proposed model, illustrating that the associative complexes could modify the rheological properties of FG.

Acknowledgements

The authors would like to acknowledge the funding support from Fujian Putian Sea-100 Food Co., Ltd (R-143-000-633-597).

Appendix A. Properties of raw materials

Table A.1
Characteristics of raw materials.

Sample	$\overline{M_v}$ (g/mol)[a]	pI	Metal ions, dry basis % (w/w)[b]		
			Ca	K	Na
FG	47,765	7.52	0.03	N.D.	N.D.
PG	29,617	7.92	0.04	N.D.	N.D.
KC	78,488	N.A.	0.39	4.94	0.31

[a]Viscosity averaged molecular weight ($\overline{M_v}$) was determined from the intrinsic viscosity and Mark-Hounwink equation, $\ln \eta = \ln k + a \ln M_w$, where the constant k and a for gelatin were 1.514 × 10–3 and 0.885, respectively (Bohidar, 1998), for KC were 7.48 × 10–3 and 0.91, respectively (Vreeman et al., 1980).
[b]Metal ions analysis was performed using inductive coupled plasma-optical emission spectroscopy (ICP-OES). The dry samples were digested with HNO3 at 240 °C in microwave for 15 min (Sow et al., 2018).
*N.A. indicates not applicable, N.D. indicates not detected.

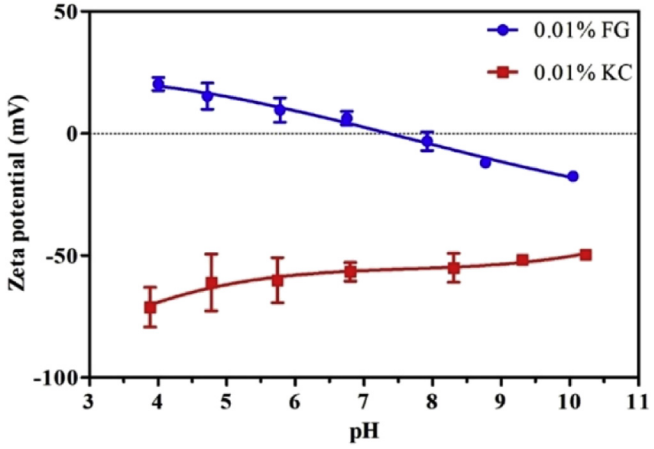

Fig. A.1. Changes of FG and KC zeta potential at various pHs.
*The isoelectric point of FG was determined to be pH 7.52.

Appendix B. Creep-recovery (Burgers model)

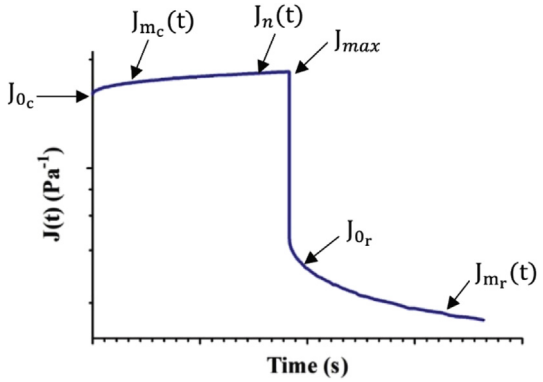

Fig. B.1. Creep-recovery curve and the Burgers model parameters.

*Creep phase,

$$J(t)_c = J_{0_c} + J_{m_c}(t) + J_n(t) \tag{B.1}$$

where viscoelastic compliance,

$$J_{m_c}(t) = \sum_{i=1}^{3} \left[J_{m_{ic}} \left(1 - e^{\frac{-t}{\lambda_{ic}}} \right) \right] \tag{B.2}$$

and Newtonian compliance,

$$J_n(t) = \frac{t}{\eta_0} \tag{B.3}$$

*Recovery phase,

$$J(t)_r = J_{max} - J_{0_r} - J_{m_r}(t) \tag{B.4}$$

Where viscoelastic compliance,

$$J_{m_r}(t) = \sum_{i=1}^{3} \left[J_{m_{i_r}} \left(1 - e^{\frac{-t}{\lambda_{i_r}}} \right) \right] \tag{B.5}$$

Appendix C. Supplementary results

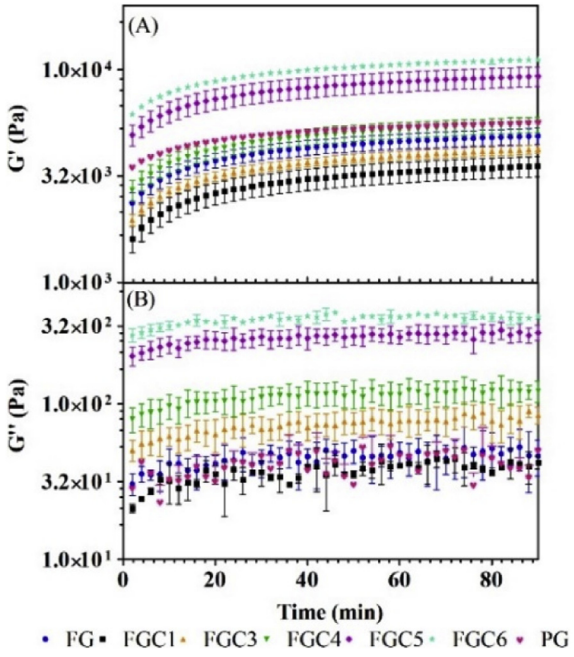

Fig. C.1. Storage modulus (G′) and loss modulus (G″) of FG, FG-KC mixtures and PG gel (6.67%) over time at 10 °C. *FGC1, FGC3, FGC4, FGC5, and FGC6 refer to FG-KC mixture with mixing ratio (KC: FG, w/w) of 0.5:99.5, 2:98, 4:96, 8:92, and 10:90, respectively. FG, fish gelatin; KC, κ-carrageenan; PG, porcine gelatin.

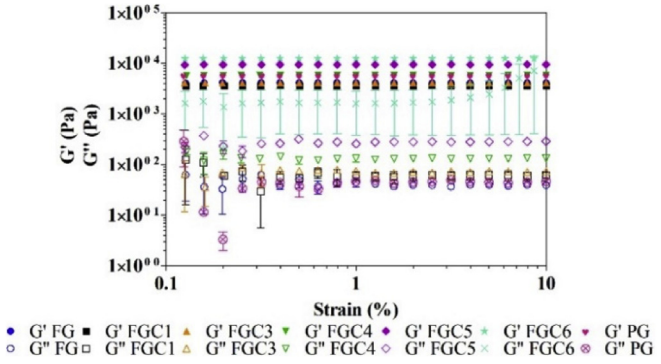

Fig. C.2. Strain sweep (0.1–10 Hz) of FG, FG-KC mixtures and PG gel (6.67%) at 10 °C, 1 Hz *FGC1, FGC3, FGC4, FGC5, and FGC6 refer to FG-KC mixture with mixing ratio (KC: FG, w/w) of 0.5:99.5, 2:98, 4:96, 8:92, and 10:90, respectively. FG, fish gelatin; KC, κ-carrageenan; PG, porcine gelatin.

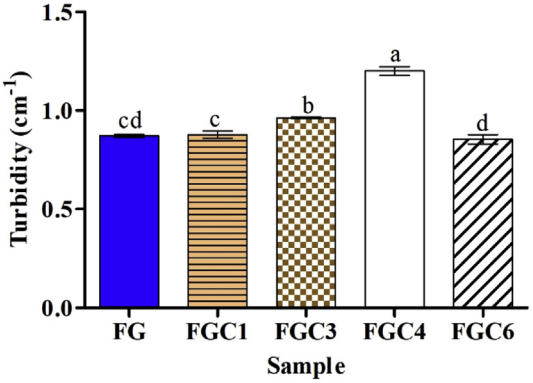

Fig. C.3. Turbidity of FG-KC gel (6.67%, w/v) at 25 °C. *FGC1, FGC3, FGC4, and FGC6 refer to FG-KC mixture with mixing ratio (KC: FG, w/w) of 0.5:99.5, 2:98, 4:96, and 10:90, respectively. FG, fish gelatin; KC, κ-carrageenan; PG, porcine gelatin.

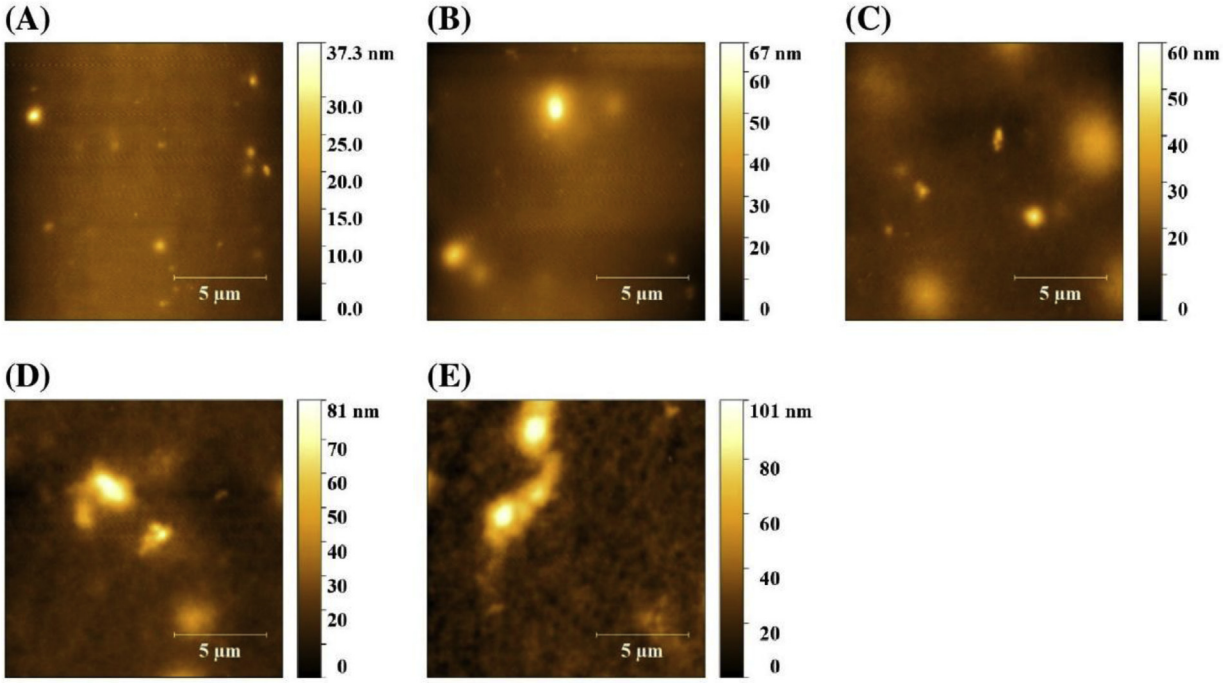

Fig. C.4. AFM of 6.67% (w/v) gel samples of (A) FG, (B) FGC1, (C) FGC3, (D) FGC4, and (E) FGC6. *FGC1, FGC3, FGC4, and FGC6 refer to FG-KC mixture with mixing ratio (KC: FG, w/w) of 0.5:99.5, 2:98, 4:96, and 10:90, respectively. FG, fish gelatin; KC, κ-carrageenan.

References

Anvari, M., Chung, D., 2016. Dynamic rheological and structural characterization of fish gelatin – gum Arabic coacervate gels cross-linked by tannic acid. Food Hydrocolloids 60, 516–524. https://doi.org/10.1016/j.foodhyd.2016.04.028.

Bohidar, H.B., 1998. Hydrodynamic properties of gelatin in dilute solutions. Int. J. Biol. Macromol. 23 (1), 1–6. https://doi.org/10.1016/S0141-8130(98)00003-8.

Cao, Y., Wang, L., Zhang, K., Fang, Y., Nishinari, K., Phillips, G.O., 2015. Mapping the complex phase behaviors of aqueous mixtures of κ-carrageenan and type B gelatin. J. Phys. Chem. B 119 (30), 9982–9992. https://doi.org/10.1021/acs.jpcb.5b05002.

Chen, L., Zhou, Y., He, Z., Liu, Q., Lai, S., Yang, H., 2018. Effect of exogenous ATP on the postharvest properties and pectin degradation of mung bean sprouts (*Vigna radiata*). Food Chem. 251, 9–17. https://doi.org/10.1016/j.foodchem.2018.01.061.

Chourpa, I., Ducel, V., Richard, J., Dubois, P., Boury, F., 2006. Conformational modifications of α gliadin and globulin proteins upon complex coacervates formation with gum Arabic as studied by Raman microspectroscopy. Biomacromolecules 7 (9), 2616–2623. https://doi.org/10.1021/bm060131d.

Derkach, S.R., Ilyin, S.O., Maklakova, A.A., Kulichikhin, V.G., Malkin, A.Y., 2015. The rheology of gelatin hydrogels modified by κ-carrageenan. LWT - Food Sci. Technol 63 (1), 612–619. https://doi.org/10.1016/j.lwt.2015.03.024.

Derkach, S.R., Voron'ko, N.G., Maklakova, A.A., Kondratyuk, Y.V., 2014. The rheological properties of gelatin gels containing κ-carrageenan. The role of polysaccharide. Colloid J. 76 (2), 146–152. https://doi.org/10.1134/S1061933X14020021.

Du, L., Brenner, T., Xie, J., Matsukawa, S., 2016. A study on phase separation behavior in kappa/iota carrageenan mixtures by micro DSC, rheological measurements and simulating water and cations migration between phase. Food Hydrocolloids 55, 81–88. https://doi.org/10.1016/j.foodhyd.2015.11.004.

Fang, Y., Li, L., Inoue, C., Lundin, L., Appelqvist, I., 2006. Associative and segregative phase separations of gelatin/κ-carrageenan aqueous mixtures. Langmuir 22 (23), 9532–9537. https://doi.org/10.1021/la061865e.

Feng, X., Bansal, N., Yang, H., 2016. Fish gelatin combined with chitosan coating inhibits myofibril degradation of golden pomfret (*Trachinotus blochii*) fillet during cold storage. Food Chem. 200, 283–292. https://doi.org/10.1016/j.foodchem.2016.01.030.

Feng, X., Fu, C., Yang, H., 2017a. Gelatin addition improves the nutrient retention, texture and mass transfer of fish balls without altering their nanostructure during boiling. LWT-Food Sci. Technol. 77, 142–151. https://doi.org/10.1016/j.lwt.2016.11.024.

Feng, X., Ng, V.K., Mikš-Krajnik, M., Yang, H., 2017b. Effects of fish gelatin and tea polyphenol coating on the spoilage and degradation of myofibril in fish fillet during cold storage. Food Bioprocess Technol. 10 (1), 89–102. https://doi.org/10.1007/s11947-016-1798-7.

Fu, Z., Che, L., Li, D., Wang, L., Adhikari, B., 2016. Effect of partially gelatinized corn starch on the rheological properties of wheat dough. LWT - Food Sci. Technol. 66, 324–331. https://doi.org/10.1016/j.lwt.2015.10.052.

Haug, I.J., Draget, K.I., Smidsrød, O., 2004. Physical behaviour of fish gelatin-κ-carrageenan mixtures. Carbohydr. Polym. 56 (1), 11–19. https://doi.org/10.1016/j.carbpol.2003.10.014.

Karim, A.A., Bhat, R., 2009. Fish gelatin: properties, challenges, and prospects as an alternative to mammalian gelatins. Food Hydrocolloids 23 (3), 563–576. https://doi.org/10.1016/j.foodhyd.2008.07.002.

Kitade, Y., Miyabe, Y., Yamamoto, Y., Takeda, H., Shimizu, T., Yasui, H., Kishimura, H., 2017. Structural characteristics of phycobiliproteins from red alga *Mazzaella japonica*. J. Food Biochem. 42 (1), e12436. https://doi.org/10.1111/jfbc.12436.

Liu, S., Wang, Y., 2011. Chapter 6-A review of the application of atomic force microscopy (afm) in food science and technology. In: Steve, L.T. (Ed.), Advances in Food and Nutrition Research. Academic Press, pp. 201–240. https://doi.org/10.1016/B978-0-12-385989-1.00006-5.

Messens, W., Van de Walle, D., Arevalo, J., Dewettinck, K., Huyghebaert, A., 2000. Rheological properties of high-pressure-treated gouda cheese. Int. Dairy J. 10 (5), 359–367. https://doi.org/10.1016/S0958-6946(00)00066-2.

Moreira, R., Chenlo, F., Torres, M.D., Prieto, D.M., 2010. Influence of the particle size on the rheological behaviour of chestnut flour doughs. J. Food Eng. 100 (2), 270–277. https://doi.org/10.1016/j.jfoodeng.2010.04.009.

Nakauma, M., Funami, T., Fang, Y., Nishinari, K., Draget, K.I., Phillips, G.O., 2016. Calcium binding and calcium-induced gelation of sodium alginate modified by low molecular-weight polyuronate. Food Hydrocolloids 55, 65–76. https://doi.org/10.1016/j.foodhyd.2015.10.021.

Pang, Z., Deeth, H., Prakash, S., Bansal, N., 2016. Development of rheological and sensory properties of combinations of milk proteins and gelling polysaccharides as potential gelatin replacements in the manufacture of stirred acid milk gels and yogurt. J. Food Eng. 169, 27–37. https://doi.org/10.1016/j.jfoodeng.2015.08.007.

Pang, Z., Deeth, H., Yang, H., Prakash, S., Bansal, N., 2017. Evaluation of tilapia skin gelatin as a mammalian gelatin replacer in acid milk gels and low-fat stirred yogurt. J. Dairy Sci. 100 (5), 3436–3447. https://doi.org/10.3168/jds.2016-11881.

Pranoto, Y., Lee, C.M., Park, H.J., 2007. Characterizations of fish gelatin films added with gellan and κ-carrageenan. LWT - Food Sci. Technol. 40 (5), 766–774. https://doi.org/10.1016/j.lwt.2006.04.005.

Razzak, M.A., Kim, M., Chung, D., 2016. Elucidation of aqueous interactions between fish gelatin and sodium alginate. Carbohydr. Polym. 148, 181–188. https://doi.org/10.1016/j.carbpol.2016.04.035.

Robal, M., Brenner, T., Matsukawa, S., Ogawa, H., Truus, K., Rudolph, B., Tuvikene, R., 2017. Monocationic salts of carrageenans: preparation and physico-chemical properties. Food Hydrocolloids 63, 656–667. https://doi.org/10.1016/j.foodhyd.2016.09.032.

Sow, L.C., Kong, K., Yang, H., 2018. Structural modification of fish gelatin by the addition of gellan, κ-carrageenan, and salts mimics the critical physicochemical properties of pork gelatin. J. Food Sci. 83 (5), 1280–1291. https://doi.org/10.1111/1750-3841.14123.

Sow, L.C., Peh, Y.R., Pekerti, B.N., Fu, C., Bansal, N., Yang, H., 2017. Nanostructural analysis and textural modification of tilapia fish gelatin affected by gellan and calcium chloride addition. LWT - Food Sci. Technol. 85, 137–145. https://doi.org/10.1016/j.lwt.2017.07.014.

Sow, L.C., Yang, H., 2015. Effects of salt and sugar addition on the physicochemical properties and nanostructure of fish gelatin. Food Hydrocolloids 45, 72–82. https://doi.org/10.1016/j.foodhyd.2014.10.021.

van Riemsdijk, L.E., Snoeren, J.P.M., van der Goot, A.J., Boom, R.M., Hamer, R.J., 2010. Particle size effects in colloidal gelatin particle suspensions. J. Food Eng. 101 (4), 394–401. https://doi.org/10.1016/j.jfoodeng.2010.07.025.

Voron'ko, N.G., Derkach, S.R., Vovk, M.A., Tolstoy, P.M., 2016. Formation of κ-carrageenan–gelatin polyelectrolyte complexes studied by 1H NMR, UV spectroscopy and kinematic viscosity measurements. Carbohydr. Polym. 151, 1152–1161. https://doi.org/10.1016/j.carbpol.2016.06.060.

Voron'ko, N.G., Derkach, S.R., Vovk, M.A., Tolstoy, P.M., 2017. Complexation of κ-carrageenan with gelatin in the aqueous phase analysed by 1H NMR kinetics and relaxation. Carbohydr. Polym. 169, 117–126. https://doi.org/10.1016/j.carbpol.2017.04.010.

Vreeman, H.J., Snoeren, T.H.M., Payens, T.A.J., 1980. Physicochemical investigation of k-carrageenan in the random state. Biopolymers 19 (7), 1357–1374. https://doi.org/10.1002/bip.1980.360190711.

Wang, Y., Yang, H., Regenstein, J., 2008. Characterization of fish gelatin at nanoscale using atomic force microscopy. Food Biophys. 3 (2), 269–272. https://doi.org/10.1007/s11483-008-9083-6.

Yang, Z., Yang, H., Yang, H., 2018. Effects of sucrose addition on the rheology and microstructure of κ-carrageenan gel. Food Hydrocolloids 75, 164–173. https://doi.org/10.1016/j.foodhyd.2017.08.032.

Yilmaz, M.T., Karaman, S., Dogan, M., Yetim, H., Kayacier, A., 2012. Characterization of O/W model system meat emulsions using shear creep and creep recovery tests based on mechanical simulation models and their correlation with texture profile analysis (TPA) parameters. J. Food Eng. 108 (2), 327–336. https://doi.org/10.1016/j.jfoodeng.2011.08.005.

Zhong, Q., Ikeda, S., 2012. Viscoelastic properties of concentrated aqueous ethanol suspensions of α-zein. Food Hydrocolloids 28 (1), 46–52. https://doi.org/10.1016/j.foodhyd.2011.11.014.